Nat. Hazards Earth Syst. Sci. Discuss., 3, 1861–1887, 2015
www.nat-hazards-earth-syst-sci-discuss.net/3/1861/2015/
doi:10.5194/nhessd-3-1861-2015

Natural Hazards and Earth System Sciences
Open Access
Discussions

Large submarine earthquakes occurred worldwide, 1 year period (June 2013 to June 2014), – contribution to the understanding of tsunamigenic potential

R. Omira[1,2], **D. Vales**[1], **C. Marreiros**[1], **and F. Carrilho**[1]

[1]Instituto Português do Mar e da Atmosfera, IPMA, I. P., Lisbon, Portugal
[2]Instituto Dom Luiz, University of Lisbon, IDL, Lisbon, Portugal

Received: 19 February 2015 – Accepted: 23 February 2015 – Published: 11 March 2015

Correspondence to: R. Omira (omirarachid10@yahoo.fr)

Published by Copernicus Publications on behalf of the European Geosciences Union.

Abstract

This paper is a contribution to a better understanding of tsunamigenic potential from large submarine earthquakes. Here, we analyse the tsunamigenic potential of large earthquakes occurred worldwide with magnitudes around M_w 7.0 and greater, during a period of 1 year, from June 2013 to June 2014. The analysis involves earthquake model evaluation, tsunami numerical modelling, and sensors' records analysis in order to confirm the generation or not of a tsunami following the occurrence of an earthquake. We also investigate and discuss the sensitivity of tsunami generation to the earthquake parameters recognized to control the tsunami occurrence, including the earthquake magnitude, focal mechanism and fault rupture depth. A total of 23 events, with magnitudes ranging from M_w 6.7 to M_w 8.1 and hypocenter depths varying from 10 up to 585 km, have been analyzed in this study. Among them, 52 % are thrust faults, 35 % are strike-slip faults, and 13 % are normal faults. Most analyzed events have been occurred in the Pacific Ocean. This study shows that about 39 % of the analyzed earthquakes caused tsunamis that were recorded by different sensors with wave amplitudes varying from few centimetres to about 2 m. Some of them caused inundations of low-lying coastal areas and significant damages in harbours. On the other hand, tsunami numerical modeling shows that some of the events, considered as non-tsunamigenic, might trigger small tsunamis that were not recorded due to the absence of sensors in the near-field areas. We also find that the tsunami generation is mainly dependent of the earthquake focal mechanism and other parameters such as the earthquake hypocenter depth and the magnitude. The results of this study can help on the compilation of tsunami catalogs.

1 Introduction

In the aftermath of the 2004 Indian Ocean tsunami, many efforts have been addressed worldwide to better understand the potential of tsunami generation following the occur-

NHESSD
3, 1861–1887, 2015

rence of an earthquake. As results, various research works have been performed in order to: (i) identify the source zones mostly prone to trigger tsunami around the world, (ii) understand the generation mechanism of tsunami sources, (iii) assess tsunami hazard, vulnerability, and risk along the coastal areas, (vi) reinforce the existing tsunami warning systems (TWSs) and implement new ones, (v) improve the capability of tsunami warning centres (TWCs) to detect the tsunami well before it hits the coastal zones. One issue that remains challenging for any TWC, in order to avoid false warning and mitigate the tsunami impact on coastal population, is the fast confirmation of a generation or not of a tsunami after the occurrence of an earthquake. Solving such an issue, in particular with the absence of tsunami detection sensors deployed close to the earthquake epicentre, remains a hard task and requires robust knowledge on the geology, tectonic, and geodynamic of the region where the earthquakes are generated in addition to robust tsunami numerical modelling capabilities able to simulate properly the different phases of a tsunami.

In general, various parameters are recognized to control the generation of a tsunami following an earthquake event. These parameters mainly include the earthquake magnitude, its location, its focal mechanism, and its rupture depth. Available tsunami database from 2000 BC to present (NGDC/WDS, 2014) shows that among the total of 1425 tsunami historical events 80 % were caused by earthquakes of magnitude greater than M_w 6.5. Most, but not all, known devastating tsunamis has been caused by earthquakes triggered in subduction zones. According to Satake and Tanioka (1999), tsunamigenic earthquakes in subduction zones can be classified into three types: (i) typical interpolate events, which occurred at the plate interface, (ii) interpolate events concerning earthquakes at the outer rise within the subducting slab or overlying crust; and (iii) "tsunami earthquakes" that take place at the shallow extension of the interplate seismogenic zone, typically beneath the accretionary wedge.

This study aims to contribute to a better understanding of tsunamigenic potential from sources of tectonic origin by analyzing the tsunami generation from big events occurred worldwide during a period of 1 year. 23 submarine earthquake events of mag-

NHESSD
3, 1861–1887, 2015

nitudes ranging from M_w 6.7 up to M_w 8.1 have been analysed (Fig. 1). Most considered events have occurred in the Pacific Ocean on/or near the plate subduction zones. These events took places with different focal mechanisms of generation and different earthquake hypocenter depths.

The analysis involves source parameters evaluation, tsunami numerical modelling of generation and propagation, and sensors (tides gauges (TD), and deep ocean assessment and reporting of tsunamis (DART)) records that serve to confirm the generation or not of a tsunami. Definition of source parameters includes the earthquake epicentre location (from USGS), its magnitude, its depth, and its focal mechanism, which are available by the gCMT (Global Centroid–Moment–Tensor, http://www.globalcmt.org/) after the event occurrence. To evaluate the additional parameters, such as the fault dimensions (L, W) and the co-seismic slip (S), required for tsunami numerical modelling, we use the earthquakes scaling laws M_w L/W and M_w S established by Blaser et al. (2010). To simulate the possible initial sea-surface perturbation, the earthquake rupture is supposed instantaneous and the sea-bed displacement is computed using the half-space elastic theory (Okada, 1985). The tsunami propagation is modelled using a validated finite-differences shallow water model.

Analysis of available sensors'records reveals that 39 % of the considered earthquakes caused tsunami. We show that the tsunami generation from those events is mainly dependent of various specific characteristics of earthquake mechanism generation, such as the earthquake magnitude, the type of the focal mechanism, and the depth of the rupture. 67 % of caused tsunamis resulted from thrust faults occurred in/or near subduction zones. We finally discuss the performance of the different TWS around the world to the triggered tsunami events.

2 Earthquake events: tectonic setting and focal mechanisms

In this study 23 large submarine earthquakes, occurred between June 2013 and June 2014, have been considered. Most analyzed events resulted from thrust faults

NHESSD
3, 1861–1887, 2015

located on/or near the plate subduction zones in the Pacific Ocean. These subductions include New Britain Trench, Aleutians Arc, South Sandwich Trench, Peru-Chile trench, Philippine Trench, Japan Trench, Kuril-Kamchatka Trench, Cascadia Subduction and Middle-American Trench. We also studied in the Mediterranean Sea an event associated with the Hellenic arc. On the other hand, some of the considered events were associated with strike-slip motion and occurred in the Atlantic Ocean, Pacific Ocean, and Mediterranean Sea.

Assessing the tsunamigenic potential of the studied earthquakes requires an understanding of the tectonic setting of the regions where these events have occurred. Here, we describe the tectonic setting of these regions and the focal mechanism responsible of each earthquake. We consider four main source zones as responsible for the generation of events considered in this study. They are: the west Pacific, the east Pacific, the south Atlantic and the west Mediterranean source zones.

Figure 2 depicts the events occurred in the west Pacific source zone. Figure 2a presents an overview of the west Pacific source zone. In Fig. 2b–e, we plot the focal mechanisms of the studied earthquakes in the west Pacific source zones that have magnitudes ranging from M_w 6.7 to M_w 7.6. These events took place in the Sea of Okhotsk – Russia (Fig. 2b), in the Aleutian Islands region (Fig. 2c), offshore Honshu – Japan (Fig. 2d), in the Bohol Islands–Philippines (Fig. 2e), and in Papua New Guinea and Solomon Islands regions (Fig. 2f).

In the Sea of Okhotsk, the 1 October 2013, a M_w 6.7 earthquake was the result of normal faulting at a depth of 585 Km (Fig. 2b). Its location is close to the region where the Pacific Plate subducts beneath the Okhotsk Plate (part of the North American plate) (Fig. 2b). The Pacific plate is moving towards the northwest in relation to the North America plate at a rate of 75 mm yr^{-1} near the northern end of the arc and at 83 mm year^{-1} in the south. The Kuril Island chain and the deep offshore Kuril-Kamchatka Trench (200 km east) (Fig. 2b) are the result of this subduction (Rhea et al., 2010). This is one of the few regions in the world where strong earthquakes happen at such great depths. In the Aleutian Islands region, took place on 30 August 2013

NHESSD
3, 1861–1887, 2015

a M_w 7.0 earthquake at a depth of 26.7 km (Fig. 2c), as the result of thrust faulting on/near the subduction zone interface between the Pacific and North America plates, the Aleutian trench (Fig. 2c). Near the hypocenter the Pacific plate moves towards the northwest with respect to North America at a rate of $\sim 73\,\mathrm{mm\,yr^{-1}}$, roughly 130 km north of the Aleutian trench. The Aleutian Arc, marking the region where the Pacific plate subducts into the mantle beneath the North America plate (Benz et al., 2011a), extends approximately 3000 km from the Gulf of Alaska in the east to the Kamchatka Peninsula in the west. Offshore of Honshu, Japan, occurred a M_w 7.1 earthquake on 25 October 2013, associated with a normal faulting in oceanic crust of the Pacific plate, east of the Japan Trench (Fig. 2d). In this subduction zone along the boundary between the Pacific and North America plates, the Pacific plate moves westwards with respect to the North America plate at a rate of $\sim 83\,\mathrm{mm\,yr^{-1}}$. This earthquake is immediately up-dip of the source region of the March 2011 M_w 9.0 Tohoku earthquake. In the Bohol Islands, Philippines, a M_w 7.1 earthquake happened on 15 October 2013 (Fig. 2e) as origin of an unmapped reverse fault (Lagmay and Eco, 2014). The depth of the event (12 km) indicates that it ruptured a fault within the crust of the Sunda plate, rather than on the deeper subduction zone plate boundary interface (the Philippine Trench) (from USGS). The Philippine Sea plate is bordered by the Pacific, Eurasia and the Sunda plates and it moves towards the west-northwest relative to the Sunda plate at a rate of $\sim 10\,\mathrm{cm\,yr^{-1}}$, the subduction happens a few hundred kilometres to the east of the 15 October earthquake at the Philippine Trench. Four events have occurred in the Papua New Guinea (Fig. 2f) within two tectonic regions, namely the Australia slab and the New Britain Trench. The Australia slab, northeast of Papua New Guinea, is seismically active to depths of over 400 km. This region was responsible for the generation of a M_w 7.3 earthquake in 7 July 2013 that is associated with normal faulting at 385 km depth. Not far to the south (~ 200 km) is the New Britain Trench (see Fig. 2f), one of the most seismically active regions in the world, where the Australia Plate is being subducted beneath the Pacific plate at a convergence rate of $\sim 110\,\mathrm{mm\,yr^{-1}}$ (DeMets et al., 1994). Three other earthquakes (see Fig. 2e) were the result of thrust faulting on

NHESSD
3, 1861–1887, 2015

the Australia–Pacific subduction zone, close to New Britain Trench. These events took place on 16 October 2013, 11 April 2014, and 16 April 2014 with magnitudes M_w 6.8, M_w 7.1 and M_w 7.5 at depths of 45.8, 44.1 km and, 36 km, respectively. In the Solomon Islands region two earthquakes happened on 12 April 2014, and 13 April 2014 with magnitudes M_w 7.6 and M_w 7.4, respectively, along a segment of the Australia–Pacific plate boundary (Fig. 2f). This plate boundary is characterized by transitions from thrust to transform tectonics between the New Britain Trench to the northwest and the New Hebrides Trench farther east (Benz et al., 2011c). The first event was a strike-slip earthquake; while the second event, only located 20 km SW, was associated with a nearly pure reverse faulting.

Figure 3 depicts the earthquake events occurred in the west Pacific source zone. Figure 3a is an overview of the west pacific source zone where six of the studied events took place. In Fig. 3b and c we plot the focal mechanisms of the earthquake events within the west Pacific source zone of magnitudes ranging from M_w 6.7 to M_w 8.1. They have occurred off the coast of California (Fig. 3b), near the Pacific coast of Mexico (Fig. 3b), off the Peru Pacific coast (Fig. 3c), and in the northern coast of Chile (Fig. 3c).

On 10 March 2014, a M_w 6.9 earthquake occurred off the coast of northern California resulting from a strike-slip motion in a region where the Gorda plate (southernmost region of the Juan de Fuca Plate) subducts (Cascadia subduction) beneath the Pacific Northwest region at a rate of $\sim 23\,\mathrm{mm\,yr^{-1}}$ (see Fig. 3b). On a broader view, this is the region where takes place the Mendocino triple junction (located west of the California coast) of the Juan de Fuca, Pacific, and North America plates (Fig. 3b). The 18 April 2014, a M_w 7.3 earthquake happened near the Pacific coast of Mexico (Fig. 3b), as the result of thrust motion at a shallow depth (18.9 km), which is consistent with slip on or near the plate boundary interface between the subducting Cocos oceanic sea plate and the North America plate. The northeastward subduction of the Cocos plate beneath the North America plate is moving at a rate of $\sim 65\,\mathrm{mm\,yr^{-1}}$. The Mexico region is one of the world's most seismically active regions, laying above three large tectonic plates, Pacific, Cocos and North American plates (Benz et al., 2011b). On 25

NHESSD
3, 1861–1887, 2015

September 2013 a M_w 7.0 earthquake occurred off the coast of Peru at 46.1 km depth as thrust-faulting on/near the thrust interface at the boundary between the South America and the subducting Nazca plate (Fig. 3c). The Nazca plate subducts beneath the South America plate at the Peru–Chile trench offshore of western South America. Near the earthquake location, the Nazca plate moves to the east-northeast with respect to the South America plate at a convergence rate of 80 mm yr^{-1} (Angermann et al., 1999). In Northern Chile, three earthquakes resulting of thrust faulting, at shallow depths 12, 21.6 and 28.7 km, occurred near off the Chilean coast (Fig. 3c). The first event, on 16 March 2014, with M_w 6.7 was considered as a foreshock of the 1 April 2014 M_w 8.1 event and the 3 April 2014 M_w 7.7 event was an aftershock. All these earthquakes originated in the subduction zone along which Nazca plate underthrusts the South America plate (Lay et al., 2014) moving at a rate of $\sim$ 65 mm yr^{-1} (DeMets et al., 2010). The region of Iquique is known as responsible for the 1877 earthquake, or the Iquique seismic gap (Lay et al., 2014).

Figure 4 depicts the events occurred in the south Atlantic source zone. Figure 4a presents an overview of the south Atlantic source zone. In Fig. 4b, we plot the location and focal mechanisms of five earthquakes with magnitudes ranging from M_w 6.8 to M_w 7.8 with epicentres located around Bouvet Islands, Scotia plate in South Sandwich Islands, Scotia Sea and Southwest of the Falkland Islands regions.

At the South Sandwich Islands one strike-slip event occurred in 15 July 2013 with M_w 7.3 magnitude, originated at 21.5 km depth, approximately 100 km east of the triple junction between South America, Sandwich and Antarctica plates (Fig. 4b). The South America plate currently subducts beneath the Sandwich plate at a rate around 13 mm yr^{-1} while sliding past the Antarctica plate with left-lateral motion along the South Sandwich Fracture Zone at a rate of $\sim$ 14 mm yr^{-1} (DeMets, 2011). In the South Scotia Ridge Transform (SSRT) plate boundary, between the Scotia and Antarctic plates, two large strike-slip events took place on 16 November and 17 2013. The first one was a M_w 6.9 event magnitude that occurred at a shallow depth of 10 km. The second one, occurred at a depth of 23.8 km, presents the largest strike-slip earthquake,

NHESSD
3, 1861–1887, 2015

known to date, along this plate boundary (M_w 7.8) (Fig. 4b). The Antarctica plate moves eastward with respect to the Scotia Sea plate at a velocity of ~ 6–7 mm yr^{-1} (DeMets et al., 2010). Southwest of the Falkland Islands, a strike-slip faulting M_w 6.9 earthquake happened on 25 November 2013, near the boundary of the South America plate and the Scotia Sea plate (Fig. 4b). These plates slide past each other at a rate of ~ 9.9 mm yr^{-1} in an ENE direction (from USGS). On 15 April 2014 a M_w 6.8 earthquake occurred in the south Atlantic Ocean to the east of Bouvet Island resulting from strike-slip motion (Fig. 4b). About 250 km to the west of Bouvet Island we find the Bouvet Triple Junction where the boundaries of the African, South American and Antartic Plates meet (Fig. 4b). The most prominent features in the region are the Conrad and the Bouvet Fracture zones. The Mid-Atlantic Ridge (MAR) separates the African Plate and the South American Plate in the South Atlantic. The velocity rate of spreading-center of southernmost segments of the MAR is about of 30.5 mm yr^{-1} for the last 9 my (Marco et al., 1999).

Figure 5 depicts the events occurred in the western Mediterranean source zone. Figure 5a presents an overview of the western Mediterranean source zone where two earthquakes struck Greece. In Fig. 5b we display the focal mechanisms of these events of magnitudes M_w 6.8 and M_w 6.9. They both have occurred in the Aegean Sea (Fig. 5b).

The M_w 6.8 earthquake, happened on 12 October 2013 about 30 km west of Platanos, Greece, was associated with a reverse motion near the Hellenic arc, the region where the Africa Plate subducts beneath the Aegean Sea Plate (Fig. 5b). The Aegean Sea Plate is moving southwest at a rate 30 ± 1 mm yr^{-1} in respect to the Eurasia Plate (McClusky et al., 2000). The M_w 6.9 earthquake occurred on 24 May 2014 was located to the south of Samothraki Island, Greece, near the Saros Trough (the eastern end of North Aegean Trough) (Fig. 5b), a region with a predominance of similar strike-slip motion earthquakes. The faults within North Aegean Trough represent the northern portion of the North Anatolian fault, where the Anatolian micro-plate is pushed by the

NHESSD
3, 1861–1887, 2015

Arabia Plate and is moving to west, in relation to the Eurasia Plate, at a rate about 25 mm yr^{-1} (from USGS).

The studied events have different focal mechanism ruptures. Within the total of 23 analyzed earthquakes, 52 % are thrust, 35 % are strike-slip, and 13 % are normal faults.

3 Tsunamigenic potential analysis

3.1 Earthquake source models

For each analysed earthquake event we compute a source model including the fault parameters required for tsunami numerical modelling. For simplification, we adopt a rectangular shape of the fault rupture, characterized by a length (L) and a width (W). We consider the M_w magnitude evaluated by the gCMT for each event and we compute the corresponding dimensions (L and W) using the scaling laws M_w L/W established by Blaser et al. (2010). In comparison with the most frequently used scaling relations of Wells and Coppersmith (1994), Blaser et al. (2010) work has the advantage of considering the subduction zone events in the database that they used to establish the earthquakes scaling relations.

Once the earthquake fault dimension (L and W) are calculated, we use the seismic moment (M_o) definition of Aki (1972) (Eq. 1) together with the $M_o - M_w$ relation defined by Kanamori and Anderson (1975) (Eq. 2) in order to calculate the earthquake slip.

$$M_o = \mu \mathrm{LWD} \quad (1)$$

$$M_w = \frac{2}{3} \log M_o - 10.7 \quad (2)$$

Table 1 summarizes the fault parameters computed for all the considered earthquake events. These parameters are used in the next section to compute the tsunami generation.

NHESSD
3, 1861–1887, 2015

3.2 Tsunami numerical modelling and comparison with records

In this section we focus on the earthquake events for which the tsunami signals were recorded; and we are interested to numerically model the resulting tsunamis in order to compare the recorded and the modeled signals.

In order to model tsunami generation and propagation a set of bathymetric/topographic grid data is generated for each region of interest where studied earthquakes took place. 30 s gridded data from the General Bathymetric Chart of the Oceans (GEBCO) are used in this study.

The initial sea surface perturbation is generated for the studied earthquakes. The earthquake fault parameters derived in Sect. 3.1 (Table 1) were used to simulate the tsunami generation. The earthquake rupture is supposed instantaneous and the seabed displacement is computed using the half-space elastic theory (Okada, 1985). The vertical sea bottom displacement is then transferred to the free ocean surface with the assumption that both deformations of sea bottom and ocean surface are equal (Kajiura, 1970).

Shallow water equations (SWEs) through the COMCOT code (Liu et al., 1998) are used to simulate the tsunami propagation. This code solves linear and non-linear SWEs using an explicit staggered leap-frog finite differences numerical scheme for linear terms and an upwind scheme for the non-linear terms (Wang, 2009). In all considered computation domains, the code employs a radiation (or absorbing) boundary conditions, which have the property that the wave motion passes from a domain to other through the boundaries with no reflections (Broeze and Van Daalen, 1992).

For all studied tsunamigenic events (39 % of the total events) we perform numerical simulations of possible tsunami generation and propagation. Here, we present modeling results for the M_w 8.1 Chile event that occurred the 1 April 2014. This event offers a good opportunity to test the reliability of the numerical model and to compare the numerical results against the tsunami signals recorded by various DART stations in the Pacific Ocean.

NHESSD
3, 1861–1887, 2015

Figure 6 depicts the results of tsunami numerical modeling for the M_w 8.1 Chile event. The results clearly indicate that a tsunami was generated with wave amplitude up to 1 m close to the source area (Fig. 6a).

Comparison of the simulated tsunami waveforms and the recorded signals from the DART sensors (Fig. 6b–d) shows relatively good agreements in terms of tsunami arrival time and maximum wave amplitudes. In Fig. 6a we plot both recorded and simulated waveforms for the DART-32401 station that is located about 290 km west from the earthquake epicentre. The analysis of the sensor record (blue curve) indicates that the DART station captured, few seconds after the event occurrence, the seismic signal due to its location relatively close to the epicentre. Few minutes after, the DART-32401 recorded the arrival of the first tsunami wave (Fig. 6b). Simulated waveform (red curve) shows a good agreement with the tsunami recorded signal for both the tsunami travel time of about 18 min and the maximum wave amplitude of about 0.25 m. Figure 6c and d depicts the comparison between the recorded and the simulated tsunami signals for both DARTs 32412 and 32413, respectively. These sensors are located 1600 and 2800 km far away from the earthquake epicentre and therefore recorded only small tsunami amplitudes (max. amplitude of about 6 cm for DART-32412, and about 3 cm for DART-32413, blue signals in Fig. 6c and d). The simulated waveforms at the locations of DART-32412 and DART-32413 (red signals in Fig. 6c and d) indicate also small recorded tsunami amplitudes, relatively in agreement with the recorded ones.

4 Discussion

4.1 Tsunami numerical modelling

Tsunami numerical modelling is a key component of any end-to-end tsunami warning system. Recent progress in numerical modeling allows estimates of tsunami generation, propagation, and coastal impact in a proper way reaching good agreements with the recorded and observed data. In this study, we have employed a validated shallow

NHESSD
3, 1861–1887, 2015

water code in order to model the tsunami propagation and then compare the simulated waveforms with those recorded by tsunami sensors.

The results of tsunami numerical modeling (Fig. 6) produced relatively good estimates of wave amplitudes and arrival times when compared with the recorded signals from DART stations. Nevertheless, the lack of precise source information (dimensions, slip) and detailed bathymetric models leads to some differences between these signals. Figure 6b–d highlights these limitations especially regarding the estimates of the wave periods and the amplitudes of the second waves. This is particularly due to the use of empirical scaling-law to estimate the earthquake fault parameters (dimensions and slip) as well as adopting an uniform slip distribution along the fault plane. Appropriate methods to constrain the fault slip distribution model require inversion of tsunami data (Fujii et al., 2011; Wei et al., 2012; Satake et al., 2013).

An et al. (2014) assessed the source model of the 1 April 2014 tsunami using the least square inversion of tsunami records from three DART stations in the Pacific Ocean. Considering this source model they were able to properly reproduce the tsunami waveforms at the stations locations using a shallow water model. Their approach is robust in constraining the earthquake source model from tsunami observations. However, for early tsunami warning purpose a fast estimate of the earthquake source is essential. Tsunami data inversion requires the use of at least the complete first wave, which leads to delays in tsunami warning dissemination that can be significant especially for local and regional events.

4.2 Tsunamigenic potential and sensitivity to earthquake parameters

In addition to the magnitude, two main parameters are recognized to control the tsunamigenic potential, namely the focal mechanism and the rupture depth. Here, we discuss the sensitivity of tsunami generation and potential to these three parameters.

The studied events occurred with magnitudes ranging from M_w 6.7 up to M_w 8.1, at depth between 10 and 585 km, with various focal mechanisms that include normal,

NHESSD
3, 1861–1887, 2015

strike-slip, and thrust faults. 39 % of these earthquakes triggered tsunamis that were confirmed from DART and/or TD records.

In order to highlight the sensitivity of tsunami potential to earthquake parameters, we plot in the Fig. 7 the observed tsunami wave heights for the different earthquake magnitudes and rupture depths, as well as the proportion of mechanism focal types for tsunamigenic events. Figure 7a depicts the observed tsunami wave amplitudes for the various earthquake magnitudes. This figure indicates that the higher wave amplitude (more than 2 m) was observed for the higher earthquake magnitude (M_w 8.1). However, not always the higher magnitude causes the higher tsunami waves, because the figure also shows that in some cases higher magnitude earthquake events (the M_w 7.6 Solomon Islands earthquake) cause less tsunami amplitudes than smaller magnitude events (the M_w 6.7 Chile earthquake). This fact clearly indicates that the event magnitude is not the only factor controlling the tsunami potential, but there are other parameters of significant importance. In Fig. 7b, we plot observed tsunami wave amplitudes for the different depths of the analyzed events. This figure shows that significant tsunamis were recorded for low depths. In Fig. 7c we plot the proportions of mechanism focal types in order to highlight the contribution of each rupture type to the tsunamigenic potential. As expected, the Fig. 7c shows clearly that most tsunami events (67 %) were due to reverse/thrust earthquake fault ruptures. This is due to the fact that the thrust/reverse ruptures are the favorite earthquake mechanisms for tsunami generation as they are able to cause a vertical displacement of the ocean bottom.

4.3 Tsunami warning

The main goal of a TWC is to provide early alerts to the endangered coastal population when a possible tsunami is generated. Depending of the severity of the occurred earthquake and the subsequent tsunami, four types of warning messages are used by the TWCs around the world including warning, advisory, watch, and information. The tsunami warning message includes, in general, information on earthquake parameters

NHESSD
3, 1861–1887, 2015

(origin time, location, depth, magnitude) as well as an evaluation of the tsunami threat in the surrounding coasts.

For the 23 earthquake events, analyzed in this paper, tsunami alerts were issued by various TWCs (international, regional, national and/or local) including the Pacific Tsunami Warning Center (PTWC), the West Coast/Alaska Tsunami Warning Center (WC/ATWC), the Japan Meteorological Agency (JMA), Joint Australian Tsunami Warning Center (JATWC), and the Indian Tsunami Early Warning Centre (ITEWC). Alert messages of warning type were issued for 30 % of these events. Warning level messages were disseminated by JMA for the M_w 7.1 earthquake that occurred in the Japan and by the PTWC for five earthquake events that occurred in Chile (M_w 8.1 and M_w 7.7), in the Solomon Islands (M_w 7.6 and M_w 7.4), and in Papua New Guinea (M_w 7.5). For the rest of the events the issued messages were of information type.

Reducing the time delay to issue the first tsunami message after the earthquake occurrence remains challenging for any early TWC. In general, for the analyzed events in this paper, the TWCs have well performed by disseminating early tsunami message within 10 min after the occurrence of the earthquakes for 75 % of the events. By gathering the tsunami warning message from the TWCs for the studied events, the proportions of the first message time delay indicate that: for 6 % of the events the first warning message was issued within 2–5 min, for about 72 % of the events within 5–10 min, and for less than 6 % of the events the warning messages were disseminated after 15 min.

5 Conclusions

This study is a contribution to a better understanding of the tsunami potential from large submarine earthquakes occurring worldwide. The study considered the preliminary parameters evaluated for the earthquake events and the tsunami recorded data and used source evaluation models together with tsunami modeling to investigate the tsunami potential. The analysis of 23 submarine earthquake events occurred worldwide with magnitudes ranging from M_w 6.7 up to M_w 8.1 leads to the following conclusions:

NHESSD
3, 1861–1887, 2015

1. Significant number of events (39 %) was tsunamigenic.
2. The earthquake depth and focal mechanism are important factors that control the tsunamigenic potential of seismic events.
3. Most tsunami events were caused by shallow earthquakes (depth < 30 km) and thrust faults that took place on/or near the subduction zones.
4. Numerical modeling of tsunami is a robust tool for wave amplitudes and tsunami travel time estimations, in spite of some limitations on source evaluation and bathymetric data.
5. TWCs around the world have performed well for the most analyzed cases as they provide first warning within 10 min for more than 75 % of the tsunami events.

In summary the present study can help on the compilation of global tsunami catalog as well as the characterization of tsunami decision matrixes for the various oceanic regions.

Acknowledgements. This work is funded by the Join Research Center (JRC) GTIMS project (Global Tsunami Information Monitoring Service), tender no. JRC/IPR/2013/G.2/13/NC, and partially by the EU project ASTARTE – Assessment, STrategy And Risk Reduction for Tsunamis in Europe. Grant 603839, 7th FP (ENV.2013.6.4-3 ENV.2013.6.4-3). The maps in this work were made using the GMT software package (Wessel and Smith, 1998) and the GBCO 30 s-arc bathymetry background.

References

An, C., Sepúlveda, I., and Liu, P. L. F.: Tsunami source and its validation of the 2014 Iquique, Chile, earthquake, Geophys. Res. Lett., 41, 3988–3994, 2014.

Aki, K.: Scaling law of earthquake source time-function, Geophys. J. Int., 31, 3–25, 1972.

Angermann, D., Klotz, J., and Reigber, C.: Space-geodetic estimation of the Nazca-South America Euler vector, Earth Planet. Sc. Lett., 171, 329–334, 1999.

NHESSD

3, 1861–1887, 2015

Benz, H. M., Dart, R. L., Villaseñor, A., Hayes, G. P., Tarr, A. C., Furlong, K. P., and Rhea, S.: Seismicity of the Earth 1900–2010 Aleutian arc and vicinity, US Geological Survey Open-File Report 2010-1083-B, available at: http://pubs.usgs.gov/of/2010/1083/b/ (last access: January 2015), 2011a.

Benz, H. M., Herman, M., Tarr, A. C., Hayes, G. P., Furlong, K. P., Villaseñor, A., Dart, R. L., and Rhea, S: Seismicity of the Earth 1900–2010 New Guinea and vicinity, US Geological Survey Open-File Report 2010-1083-H, available at: http://pubs.usgs.gov/of/2010/1083/h/ (last access: January 2015), 2011b.

Benz, H. M., Dart, R. L., Villaseñor, A., Hayes, G. P., Tarr, A. C., Furlong, K. P., and Rhea, S.: Seismicity of the Earth 1900–2010 Mexico and vicinity, US Geological Survey Open-File Report 2010-1083-F, available at: http://pubs.usgs.gov/of/2010/1083/f/ (last access: January 2015), 2011c.

Bird, P.: An updated digital model of plate boundaries, Geochem. Geophy. Geosy., 4, 1027, doi:10.1029/2001GC000252, 2003.

Blaser, L., Krüger, F., Ohrnberger, M., and Scherbaum, F.: Scaling relations of earthquake source parameter estimates with special focus on subduction environment, B. Seismol. Soc. Am., 100, 2914–2926, 2010.

Broeze, J. and Van Daalen, E. F. G.: Radiation boundary conditions for the two-dimensional wave equation from a variational principle, Math. Comput., 58, 73–82, 1992.

DeMets, C., Gordon, R. G., Argus, D. F., and Stein, S.: Effect of recent revisions to the geomagnetic reversal time scale on estimates of current plate motions, Geophys. Res. Lett., 21, 2191–2194, 1994.

DeMets, C., Gordon, R. G., and Argus, D. F.: Geologically current plate motions, Geophys. J. Int., 181, 1–80, doi:10.1111/j.1365-246X.2009.04491.x, 2010.

Fujii, Y., Satake, K., Sakai, S. I., Shinohara, and M., Kanazawa, T.: Tsunami source of the 2011 off the Pacific coast of Tohoku Earthquake, Earth Planets Space, 63, 815–820, 2011.

GEBCO, British Oceanographic Data Centre: Centenary Edition of the GEBCO Digital Atlas, published on CD-ROM on behalf of the Intergovernmental Oceanographic Commission and the International Hydrographic Organization, Liverpool, 2003.

Hanks, T. C. and Kanamori, H.: A moment magnitude scale, J. Geophys. Res., 84, 2348–2350, doi:10.1029/JB084iB05p02348, 1979.

Kajiura, K.: Tsunami source, energy and the directivity of wave radiation, B. Earthq. Res. I. Tokyo, 48, 835–869, 1970.

NHESSD
3, 1861–1887, 2015

Kanamori, H. and Anderson, D. L.: Theoretical basis of some empirical relations in seismology, B. Seismol. Soc. Am., 65, 1073–1095, 1975.
Lagmay, A. M. F. and Eco, R.: Brief Communication: On the source characteristics and impacts of the magnitude 7.2 Bohol earthquake, Philippines, Nat. Hazards Earth Syst. Sci., 14, 2795–2801, doi:10.5194/nhess-14-2795-2014, 2014.
Lay, T., Yue, H., Brodsky, E. E., and An, C: The 1 April 2014 Iquique, Chile, M_w 8.1 earthquake rupture sequence, Geophys. Res. Lett., 41, 3818–3825, 2014.
Liu, P. L.-F., Woo, S.-B., and Cho, Y.-S.: Computer programs for tsunami propagation and inundation, Technical Report, Cornell University, Ithaca, New York, USA, 1998.
Marco, L., Bonatti, E., Bortoluzzi, G., Carrara, G., Fabretti, P., Gilod, D., Peyve, A., Skolotnev, S., and Turko, N.: Bouvet triple junction in the South Atlantic: geology and evolution, J. Geophys. Res.-Sol. Ea., 104, 29365–29385, 1999.
McClusky, S., Balassanian S., Barka, A., Demir, C., Ergintav, S., Georgiev, I., Gurkan, O., Hamburger, M., Hurst, K., Kahle, H., Kastens, K., Kekelidze, G., King, R., Kotzev, V., Lenk, O., Mahmoud, S., Mishin, A., Nadariya, M., Ouzounis, A., Paradissis, D., Peter, Y., Prilepin, M., Reilinger, R., Sanli, I., Seeger, H., Tealeb, A., Toksöz, M. N., and Veis, G.: Global Positioning System constraints on plate kinematics and dynamics in the eastern Mediterranean and Caucasus, J. Geophys. Res.-Sol. Ea., 105, 5695–5719, 2000.
NGDC/WDS: National Geophysical Data Center/World Data Service: Global Historical Tsunami Database, National Geophysical Data Center, NOAA, doi:10.7289/V5PN93H7, 2014.
Okada, Y.: Surface deformation due to shear and tensile faults in a half-space, B. Seismol. Soc. Am., 75, 1135–1154, 1985.
Rhea, S., Tarr, A. C., Hayes, G., Villaseñor, A., Furlong, K. P., and Benz, H. M.: Seismicity of the Earth 1900–2007, Kuril-Kamchatka arc and vicinity, US Geological Survey Open-File Report 2010-1083-C, available at: http://pubs.usgs.gov/of/2010/1083/c/ (last access: January 2015), 2010.
Satake, K. and Tanioka, Y.: Sources of tsunami and tsunamigenic earthquakes in subduction zones, in: Seismogenic and Tsunamigenic Processes in Shallow Subduction Zones, Birkhäuser, Basel, 467–483, 1999.
Satake, K., Fujii, Y., Harada, T., and Namegaya, Y.: Time and space distribution of coseismic slip of the 2011 Tohoku earthquake as inferred from tsunami waveform data, B. Seismol. Soc. Am., 103, 1473–1492, 2013.

NHESSD
3, 1861–1887, 2015

Wang, X.: COMCOT user manual-version 1.7, School of Civil and Environmental Engineering, Cornell University Ithaca, NY 14853, USA, available at: http://ceeserver.cee.cornell.edu/pll-group/doc/COMCOT_User_Manual_v1_7.pdf (last access: December 2014), 2009.

Wei, Y., Chamberlin, C., Titov, V. V., Tang, L., and Bernard, E. N.: Modeling of the 2011 Japan tsunami: lessons for near-field forecast, Pure Appl. Geophys., 170, 1309–1331, 2013.

Wells, D. L. and Coppersmith, K. J.: New empirical relationships among magnitude, rupture length, rupture width, rupture area, and surface displacement, B. Seismol. Soc. Am., 84, 974–1002, 1994.

Wessel, P. and Smith. W. H.: New, improved version of Generic Mapping Tools released, Eos, Transactions American Geophysical Union, 79, 579–579, 1998.

Ye, L., Lay, T., Koper, K. D., Smalley, R., Rivera, L., Bevis, M. G., Zakrajsek, A. F., and Teferle, F. N.: Complementary slip distributions of the August 4 M_w 7.6 and 17 November 2013 M_w 7.8 South Scotia Ridge earthquakes, Earth Planet. Sc. Lett., 401, 215–226, 2014.

NHESSD

3, 1861–1887, 2015

Table 1. Earthquake parameters for the 23 analyzed events.

Event N°	Date	Epicenter location		Depth (km)	M_w	Location	Fault Plane	L	W	Slip
		Lat. (°)	Lon. (°)	(gCMT)			(strike, dip, rake)	(km)	(km)	(m)
1	7 Jul 2013	−3.923	153.920	382.9	7.3	Papua New Guinea	167°, 47°, −70°	77	27	1.83
2	15 Jul 2013	−60.868	−25.144	21.5	7.3	South Sandwich Islands	271°, 85°, −18°	96	19	2.21
3	30 Aug 2013	51.537	−175.230	26.7	7.0	Aleutian Islands	64°, 67°, 86°	42	23	1.24
4	25 Sep 2013	−15.838	−74.511	46.1	7.0	Peru	307°, 31°, 84°	42	23	1.61
5	1 Oct 2013	53.200	152.786	585.5	6.7	Sea of Okhotsk	293°, 40°,-44°	38	16	0.82
6	12 Oct 2013	35.514	23.252	15.	6.8	Greece	339°, 3°, 130°	32	18	0.98
7	15 Oct 2013	9.880	124.117	12.	7.1	Philippines	42°, 40°, 80°	47	25	1.54
8	16 Oct 2013	−6.446	154.931	45.8	6.8	Papua New Guinea	307°, 43°, 85°	32	18	1.04
9	25 Oct 2013	37.156	144.661	24.9	7.1	Japan	171°, 43°, −107°	60	23	1.56
10	16 Nov 2013	−60.263	−47.062	10.	6.9	Scotia Sea	96°, 66°, 2°	53	14	1.13
11	17 Nov 2013	−60.274	−46.401	23.8	7.8	Scotia Sea	102°, 44°, 3°	200	28	3.40
12	25 Nov 2013	−53.945	−55.003	16.	6.9	Falkland Islands	158°, 80°, −171°	53	14	1.34
13	10 Mar 2014	40.829	−125.134	15.	6.9	California	230°, 86°, −2°	53	14	1.27
14	16 Mar 2014	−19.981	−70.702	12.	6.7	Chile	284°, 26°, 54°	28	17	0.90
15	01 Apr 2014	−19.610	−70.769	21.6	8.1	Chile	355°, 15°, 106°	177	73	4.00
16	03 Apr 2014	−20.572	−70.502	28.7	7.7	Chile	358°, 14°, 103°	104	48	3.26
17	11 Apr 2014	−6.586	155.048	44.1	7.1	Papua New Guinea	310°, 42°, 87°	47	25	1.40
18	12 Apr 2014	−11.270	162.148	27.3	7.6	Solomon Islands	17°, 63°, 159°	149	24	3.00
19	13 Apr 2014	−11.463	162.051	37.5	7.4	Solomon Islands	91°, 43°, 77°	70	35	2.42
20	15 Apr 2014	−53.497	8.722	16.4	6.8	Bouvet Island	128°, 81°, 5°	46	13	1.19
21	18 Apr 2014	17.397	−100.972	18.9	7.3	Mexico	303°, 18, 98°	62	31	1.71
22	19 Apr 2014	−6.755	155.024	36.	7.5	Papua New Guinea	311°, 35°, 87°	80	39	2.44
23	24 May 2014	40.289	25.389	12.	6.9	Greece	73°, 85°, −177°	53	14	1.08

NHESSD
3, 1861–1887, 2015

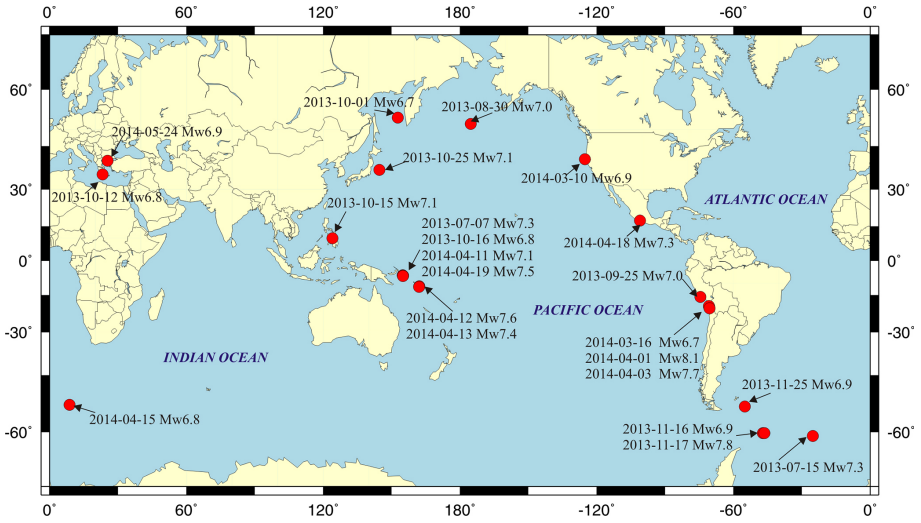

Figure 1. Locations of earthquakes (red dots), date of occurrence, and magnitudes for submarine earthquake events of $M_w \geq 6.7$ that were analyzed during a 1 year period from June 2013 to June 2014.

NHESSD
3, 1861–1887, 2015

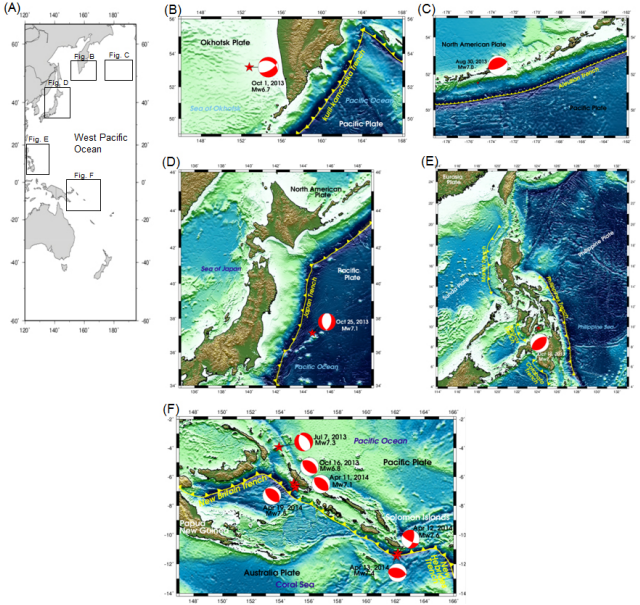

Figure 2. Earthquake events occurred in the west Pacific source zone: **(a)** overview of the source zone; **(b)** location of the Okhotsk–Russia event (red star), its focal mechanism – normal faulting (red beach ball), and the subduction zone (yellow line); **(c)** location of the Alaska event (red star), its focal mechanism – thrust fault (red beach ball), and the subduction zone (yellow line); **(d)** location of the Honshu event (red star), its focal mechanism – normal faulting (red beach ball), and the subduction zone (yellow line); **(e)** location of the Philippine event (red star), its focal mechanism – reverse faulting (red beach ball), and the subduction zone (yellow line); **(f)** locations of six events: four around the Papua New Guinea, their focal mechanisms: three are normal faulting and one is thrust faulting (red beach ball) and two near the Solomon Island (red star), their focal mechanisms: a strike-slip and a reverse faulting (red beach ball), and the subduction zone (yellow line).

NHESSD
3, 1861–1887, 2015

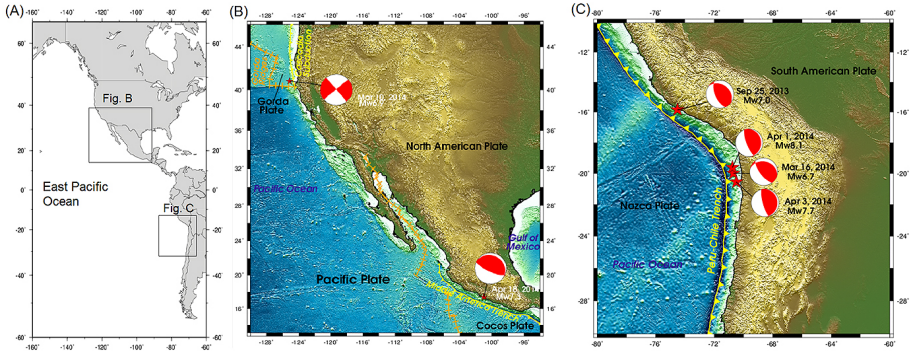

Figure 3. Earthquake events occurred in the east Pacific source zone: **(a)** overview of the source zone; **(b)** location of the California and Mexico events (red stars), their focal mechanism: thrust faulting and strike-slip faulting respectively (red beach ball), the subduction zone (yellow line) and the spreading centers (orange lines); **(c)** location of four events: the Peru event and three events in northern Chile (red stars), their focal mechanisms are thrust faulting (red beach ball), and the subduction zone (yellow line).

NHESSD
3, 1861–1887, 2015

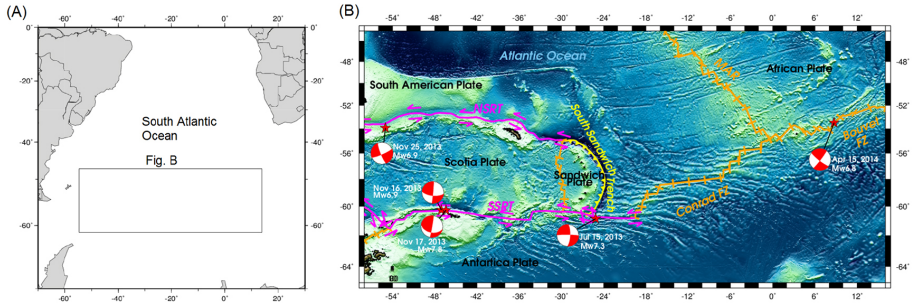

Figure 4. Earthquake events occurred in the south Atlantic Ocean source zone: **(a)** overview of the source zone; **(b)** location of five events: three around Scotia Plate, one near the Falkland Island and another one near Bouvet Island, their focal mechanisms are strike-slip faulting (red beach ball), the subduction zone (yellow line), the transforms (magenta lines), the active spreading center and fractures zones (orange lines).

NHESSD
3, 1861–1887, 2015

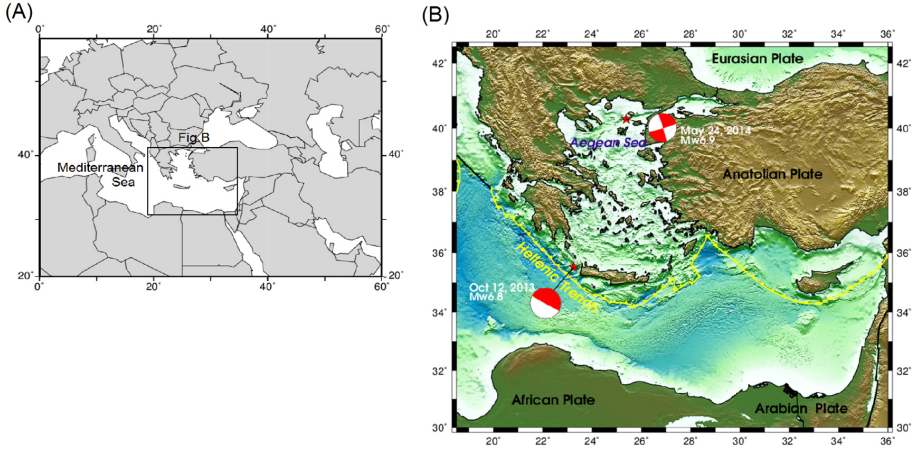

Figure 5. Earthquake events occurred in the Mediterranean source zone: **(a)** overview of the source zone; **(b)** location of the Greece events (red star), their focal mechanisms: a strike-slip faulting and a reverse faulting (red beach ball), and the subduction zone (yellow line).

NHESSD
3, 1861–1887, 2015

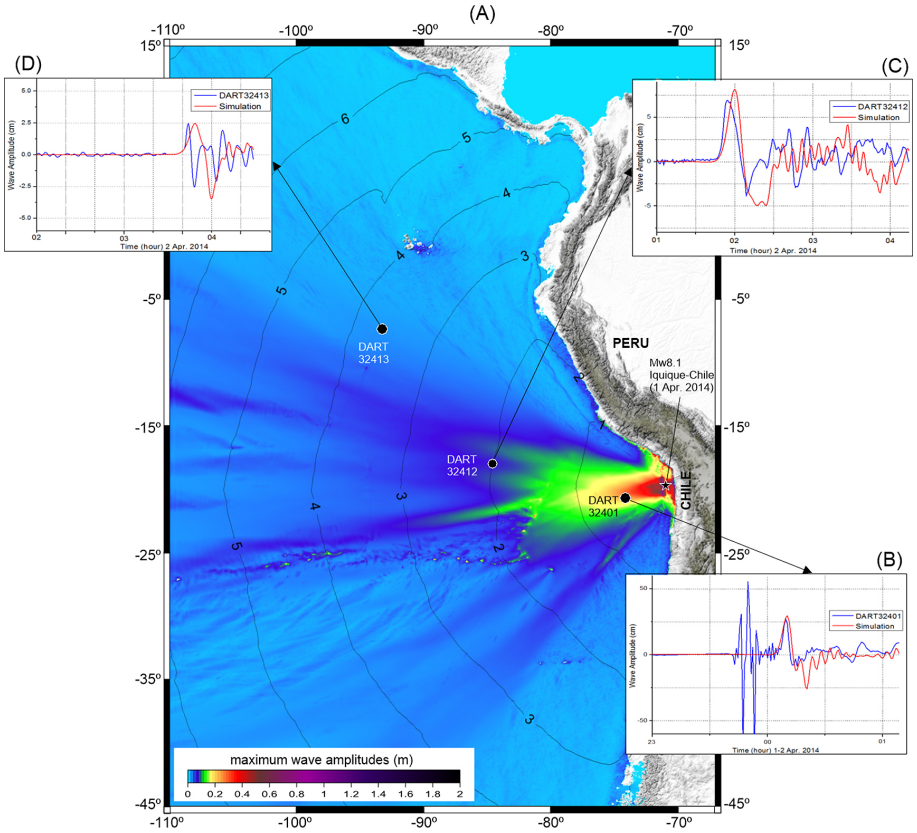

Figure 6. Tsunami numerical simulation of the 1 April 2014 Iquique–Chile tsunami event: **(a)** maximum wave amplitudes distribution in the east Pacific Ocean and tsunami travel times (dark lines separated each 1 h); **(b)** comparison between the simulated waveform and recorded signal for the station DART-32401; **(c)** comparison between the simulated waveform and recorded signal for the station DART-32412; **(d)** comparison between the simulated waveform and recorded signal for the station DART-32413.

NHESSD
3, 1861–1887, 2015

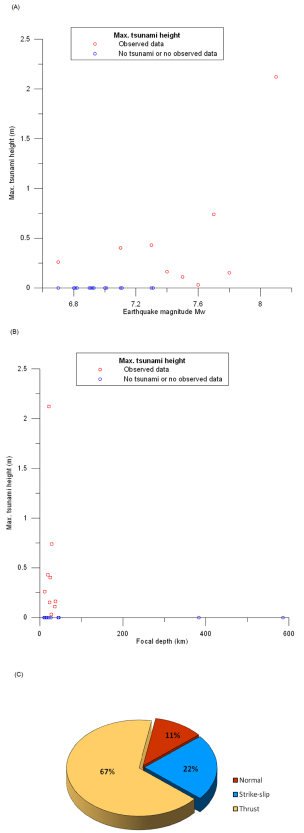

Figure 7. (a) Observed tsunami wave amplitudes for the various magnitudes of the analyzed earthquakes; **(b)** observed tsunami wave amplitudes for the different depths of the analyzed events; **(c)** proportions of mechanism focal types for the earthquake events that caused tsunamis.

NHESSD
3, 1861–1887, 2015